IMA Journal of Mathematics Applied in Medicine & Biology (1984) **1**, 51–75

Generation of Biological Pattern and Form

J. D. MURRAY

Centre for Mathematical Biology, Mathematical Institute, University of Oxford, Oxford OX1 3LB

AND

G. F. OSTER*

Department of Biophysics, University of Berkeley, Berkeley, CA 94720

[Received 15 March 1984]

We propose two models for pattern formation in early embryogenesis. The first deals with patterns in motile mesenchymal cells; the second treats patterns in epithelial sheets. In the mesenchymal model, cells exert tractions which deform the extracellular matrix within which they move. This in turn affects their motion. The model field equations are formulated and analysed, and applied to two widely studied phenomena: skin-organ primordia for feather and scale patterns, and the development of cartilage patterns in limb bone formation. The model for epithelial pattern formation consists of viscoelastic field equations with a calcium-controlled contraction trigger. Preliminary analysis is presented which demonstrates the existence of travelling wave solutions.

1. Biological background

DEVELOPMENT OF SPATIAL PATTERN and form is one of the central features of embryogenesis. Although genes certainly play a role, genetics says nothing about the actual mechanisms which produce the patterns which emerge as an organism progresses from egg to its adult form.

A variety of mathematical models have been proposed for generating pattern, the most widely studied being reaction–diffusion mechanisms (Turing, 1952; Murray, 1977; Meinhardt, 1982). In these models, 'morphogens' (chemicals) react and diffuse at different rates to produce spatially inhomogeneous patterns in morphogen concentration via the mechanism of diffusion-driven instabilities. The idea is that cells in a developing embryo respond to small concentration differences in the morphogen and execute the appropriate morphogenetic movements. While there is no doubt that chemical processes must play a central role in development, nevertheless, finding these elusive morphogens is proving remarkably difficult. There are a few cases, however, where chemically directed processes have been identified, e.g. cAMP-induced aggregation in the slime mold *Dictyostelium*; recently, Goodwin, Murray, & Baldwin (1984) have suggested that

* This work was supported by NSF grant MCS-8110557 and Science and Engineering Council of Great Britain, grant GR/C/63595.

calcium could be the morphogen in the periodic pattern of hairs in a whorl in the single-celled alga *Acetabularia*.

In this paper we take a different approach to the problem of biological pattern formation. Rather than view the morphogenesis as a 'reading out' of a chemical prepattern, we take the view that the mechanical morphogenetic movements themselves generate the pattern. The two models we propose are rooted in macroscopically measurable quantities and on generally accepted properties of embryonic cells.

In animal development the basic body plan is more or less laid down in the first few weeks (e.g. the first 4 weeks in man, and not much more in the case of a giraffe, which has a gestation period of nearly 460 days). It is during this crucial early period that we expect pattern and form generating mechanisms such as we propose here to operate.

Many morphogenetic processes involve coordinated movement of cell populations. Fibroblasts are tissue cells of particular importance: they secrete an extracellular matrix (ECM) and can generate enormous contractile forces as they crawl about. A number of factors are known to affect the movement of these embryonic cells (Trinkaus, 1983):

(a) Even during random motion, cells appear to be strongly forward biased in their movements. This is especially pronounced when cells migrate in groups.

(b) Chemotaxis, whereby cell motion is biased up or down a concentration gradient.

(c) Contact guidance, in which orientations in the substratum within which the cells crawl induce a preferred direction.

(d) Haptotaxis, where the cells move up an adhesive gradient.

(e) Galvanotaxis, in which electric fields provide a preferred direction of motion (usually toward the cathode).

(f) Contact inhibition of cell motion during encounters with other cells.

We shall describe a simple model mechanism which encapsulates these effects. We will find that regular patterned aggregates of cells can emerge from the above mechanisms, which are suggestive of certain biological patterns.

The mesenchymal cell model is based on the following important property of motile cells: cells migrating in an elastic medium (ECM) exert tractions which deform the ECM and so bias the motion of the cells (Harris, Stopak, & Wild, 1981). A preliminary version of the model is given in Murray, Oster, & Harris (1983), and a detailed biological discussion is given in Oster, Murray, & Harris (1983). While we shall not include all of the above effects which influence cell motion, it will be clear how these can easily be incorporated into the field equations and their effects assessed.

Odell, Oster, Burnside, & Alberch (1981) have shown how mechanical forces can generate morphogenetic movements in epithelial sheets. Their model is built around the notion of a contractile actomyosin fibre bundle; they construct a detailed finite-element model for an epithelial cell which can deform when chemically triggered (see Odell *et al.*, 1981). In Section 5 we shall present a continuum alternative to the finite-element model of Odell *et al.* and demonstrate the model's potential for propagation of epithelial contraction waves.

2. Field equations for mesenchymal morphogenesis

We consider a continuum model where $n(\mathbf{r}, t)$ denotes the cell density at $\mathbf{r}$. The cells migrate within an elastic matrix medium which, for simplicity, we take to be a linear elastic material. The model consists of three equations: (1) a cell conservation equation which describes the kinematics of cell motion; (2) a conservation equation for the matrix material; (3) a mechanical equation which reflects the balance of forces between the contracting cells and the elastic matrix material.

2.1 *Cell Conservation Equation*

The general form of the conservation equation is

$$\frac{\partial n}{\partial t} = -\nabla \cdot \boldsymbol{J} + M \tag{1}$$

where $\boldsymbol{J}$ is the flux of cells (number crossing a unit area in unit time), and M is the mitotic (proliferation) rate. We shall take M to be simply a logistic growth: $M = rn(N-n)$, where r is the initial proliferation rate and N the maximum cell density. We include in the flux, $\boldsymbol{J}$, the following transport effects.

(i) Convection. Let $\boldsymbol{u}(\mathbf{r}, t)$ be the displacement vector of the ECM; that is, a material point initially at position $\mathbf{r}$ undergoes a displacement to the point $\mathbf{r}+\boldsymbol{u}$. Then $n\boldsymbol{u}_t \equiv n\partial \boldsymbol{u}/\partial t$ represents the flux of cells convected along with the matrix.

(ii) Random Dispersal. Cells tend to disperse in a random way when in a homogeneous isotropic medium (we neglect the phenomenon of forward bias; it can be included by the methods discussed in Okubo (1980), Chap. 5). Classical Fickian diffusion models random motion by a flux term $\boldsymbol{J}_1 = -D_1 \nabla n$. In the present setting such a term models the response of cells to local (short range) variations in cell density. This can be seen by writing the Laplacian in the form

$$\nabla^2 n \propto [n_{\text{av}}(\mathbf{r}, t) - n(\mathbf{r}, t)]/R^2, \quad \text{as } R \to 0 \tag{2}$$

where n_{av} is the average cell concentration in a sphere of radius R and volume V, defined by:

$$n_{\text{av}} = \frac{3}{4\pi R^3} \int_V n(\mathbf{r}+\mathbf{s})\, d\mathbf{s} \tag{3}$$

If the integrand in (3) is expanded in a Taylor's series and n_{av} substituted in (2), the proportionality factor is 10/3.

In developing embryos mesodermal cells are at a fairly high density, and classical diffusion which applies to dilute systems is perhaps not sufficiently accurate. Moreover, the cells extend long filopodia which can potentially sense densities beyond nearest neighbours, and so respond to *local average density*. This non-local effect on diffusive dispersal has been considered by Othmer (1969) in the setting of chemical diffusion, and by Cohen & Murray (1981) in an ecological context. The flux of cells in such circumstances of high density becomes

$$\boldsymbol{J}_{\text{D}} = -D_1 \nabla n + D_2 \nabla^3 n \tag{4}$$

When inserted into (1) this gives rise to a biharmonic term. Note that this biharmonic diffusion term is also stabilizing if $D_2 > 0$. To see this consider the biharmonic diffusion equation

$$n_t = -\nabla \cdot \boldsymbol{J}_D = -D_2 \nabla^4 n + D_1 \nabla^2 n$$

and look for solutions of the form $n \sim e^{\lambda t + i\boldsymbol{k}\cdot\boldsymbol{r}}$, where $\boldsymbol{k}$ is any wave vector. Substituting this into the last equation gives the dispersion relation $\lambda = -D_2 k^4 - D_1 k^2 < 0$ for all wave numbers k. So $n \to 0$ as $t \to \infty$, which implies $n = 0$ is stable. Thus stability is enhanced by the biharmonic term.

(iii) Haptotaxis. The traction exerted by the cells on the matrix generates gradients in the matrix density.

We associate the density of matrix, denoted by $\rho(\boldsymbol{r}, t)$, with the density of adhesive sites for the cell lamellae to attach to. Cells free to move in an adhesive gradient tend to move up it, since the cells can get a stronger grip on the denser matrix. This results in a net flux of cells up the gradient with an average drift velocity which, on the simplest assumption, is proportional to $\nabla\rho$. Thus the haptotactic flux term has the form $\boldsymbol{J}_h = \alpha n \nabla \rho$. By the same philosophy which led us to include a nonlocal diffusion flux, we may also add a nonlocal haptotactic term. Thus the total haptotactic flux is

$$\boldsymbol{J}_h = \alpha n \nabla(\rho + \alpha' \nabla^2 \rho) \tag{5}$$

where the parameter $\alpha > 0$ and $\alpha' \leq 0$. We should mention here, however, that the inclusion of nonlocal effects are not central to the model.

With these effects the cell conservation equation (1) becomes

$$\frac{\partial n}{\partial t} = \nabla \cdot (D_1 \nabla n - D_2 \nabla^3 n) - \nabla \cdot \alpha n \nabla \rho - \nabla \cdot \left(n \frac{\partial \boldsymbol{u}}{\partial t} \right) + rn(N - n) \tag{6}$$

We have not included in (6) such effects as galvanotaxis which may well operate in developing embryos. However, it is easy to add such terms: if ϕ is the electric potential, then the galvanotactic flux can be written $\boldsymbol{J}_G = \xi n \nabla \phi$. Another effect which we shall not include in our analysis is contact guidance by directional cues in the ECM. For example, matrix strains encourage specific directions for movement as opposed to others. This can be incorporated into the equation for n by making the diffusion coefficients functions of the elastic strain tensor $\boldsymbol{\varepsilon} \equiv \frac{1}{2}[\nabla \boldsymbol{u} + (\nabla \boldsymbol{u})^T]$. The qualitative form of the dependence on $\boldsymbol{\varepsilon}$ can be deduced from experiments.

2.2 *Cell–Matrix Interaction Equation*

Since the time scale is long and the dimensions of typical developmental processes are small we can ignore inertial effects in the mechanical equation of motion. Therefore, we assume that the traction forces generated by the cells are essentially in mechanical equilibrium with the viscoelastic restoring forces developed in the matrix, and the body forces tethering the matrix material to its surroundings. The matrix consists of fibrous material whose mechanical properties have not yet been well characterized (personal communication from D. Stopak,

1983). However, as a reasonable first approximation we shall model the composite of cells and matrix as a linear, isotropic, viscoelastic material with stress tensor $\boldsymbol{\sigma}$. Thus the mechanical balance equation has the form

$$\nabla \cdot \boldsymbol{\sigma} + \rho \boldsymbol{F} = \boldsymbol{0} \tag{7}$$

where $\boldsymbol{F}$ is the vector of external forces applied to the system. $\boldsymbol{\sigma}$ can be written

$$\boldsymbol{\sigma} = \boldsymbol{\sigma}_{\text{ECM}} + \boldsymbol{\sigma}_{\text{cell}}$$

where the matrix stress tensor $\boldsymbol{\sigma}_{\text{ECM}}$ is

$$\boldsymbol{\sigma}_{\text{ECM}} = \mu_1 \boldsymbol{\varepsilon}_t + \mu_2 \theta_t \boldsymbol{I} + \frac{E}{1+\nu}(\boldsymbol{\varepsilon} + \hat{\nu}\theta \boldsymbol{I}) \tag{8a}$$

$$\boldsymbol{\sigma}_{\text{cell}} = \tau(n)(\rho + \beta \nabla^2 \rho)\boldsymbol{I}. \tag{8b}$$

Here μ_1 and μ_2 are the shear and bulk viscosities, respectively, of the ECM, $\boldsymbol{\varepsilon}$ the strain tensor, $\theta = \nabla \cdot \boldsymbol{u}$ the dilatation, E and ν the elastic modulus and Poisson ratio and β a measure of the nonlocal effect. In (8a) we have used the abbreviation $\hat{\nu} \equiv \nu/(1-2\nu)$. The term $\tau(n)$ in (8b) is the contribution to the stress from the cell tractions. Since when cells become densely packed they are inhibited from movement, and it is likely that their tractions decrease, we shall take $\tau(n)$ to be a saturating function of cell density. The actual form must be determined from experiment; here we shall use the form

$$\tau(n) = \tau n/(1+\lambda n).\dagger \tag{9}$$

Here $\tau > 0$ is a measure of the traction force generated by a cell, which can be extraordinarily large: experiments show that τ is of the order of $10^{-2}\,\text{N m}^{-1}$ of cell edge (Harris, Wild, & Stopak, 1980). If we include a nonlocal effect in $\boldsymbol{\sigma}_{\text{cell}}$ we write

$$\boldsymbol{\sigma}_{\text{cell}} = \rho[\tau/(1+\lambda n)](n + \gamma \nabla^2 n)\boldsymbol{I}$$

where γ measures the magnitude of the nonlocal effect. Inclusion of this nonlocal effect is probably more important than the corresponding term in the motility equation.

$\boldsymbol{F}$ in equation (7) represents the body forces on the matrix–cell system. In the applications we have in mind, the cell–matrix material is attached to a substratum of underlying tissue, and we shall model these restraining forces as linear:

$$\boldsymbol{F} = -\rho s \boldsymbol{u} \tag{10}$$

where s (>0) is an elastic parameter characterizing the substrate attachments.

The force equation for the mechanical equilibrium between the cells and the ECM can now be written from (7) and (10) as

$$\nabla \cdot \left(\mu_1 \boldsymbol{\varepsilon}_t + \mu_2 \theta_t \boldsymbol{I} + \frac{E}{1+\nu}(\boldsymbol{\varepsilon} + \hat{\nu}\theta \boldsymbol{I}) + \frac{\tau n}{1+\lambda n}(\rho + \beta \nabla^2 \rho)\boldsymbol{I} \right) - s\rho \boldsymbol{u} = \boldsymbol{0} \tag{11}$$

A nonlinear effect which we have not included here is the stress alignment of the matrix fibres. This would have to be modelled by including more elastic

† Recent experimental evidence suggests that τ may decrease for n large: in this case λn^2 should replace λn.

constants. However, one effect of fibre alignment is to increase the apparent elastic modulus, an effect we can treat in the isotropic approximation by letting E be an increasing function of the dilatation, θ. We shall include this effect in the epithelial model discussed below.

2.3 *Matrix Conservation Equation*

The conservation equation for the matrix material, $\rho(\boldsymbol{r}, t)$, is

$$\partial\rho/\partial t = -\nabla\cdot(\rho\boldsymbol{u}_t) + S(n, \rho, \boldsymbol{u}) \tag{12}$$

where $S(n, \rho, \boldsymbol{u})$ is the rate cells secrete matrix material. In the following we shall consider cases wherein the secretion term can be neglected.

Equations (6), (11), and (12) constitute the model equations. The dependent variables are the density fields $n(\boldsymbol{r}, t)$, $\rho(\boldsymbol{r}, t)$ and the displacement field $\boldsymbol{u}(\boldsymbol{r}, t)$. The model involves twelve parameters: $\{D_1, D_2, \alpha, r, N, \mu_1, \mu_2, \lambda, \beta, s, E, \nu\}$. All of these are in principle measurable, and some are currently being investigated.

In order to assess the relative importance of the various effects, and for the other usual reasons, we form dimensionless equivalents of the model equations using a general length and time scale, L and T, respectively, and take the initial matrix density to be uniform at ρ_0. Then we define the following dimensionless quantities:

$$\left.\begin{aligned}
&\boldsymbol{r}^* = \boldsymbol{r}/L, && t^* = t/T, && \boldsymbol{u}^* = \boldsymbol{u}/L, && \nabla^* = L\nabla,\ \theta^* = \theta,\\
&\boldsymbol{\varepsilon}^* = \boldsymbol{\varepsilon}, && \gamma^* = \gamma/L^2, && n^* = n/N, && s^* = s\rho_0 L^2(1+\nu)/E,\\
&\alpha^* = \alpha\rho_0 T/L^2, && \beta^* = \beta/L^2, && \lambda^* = \lambda N, && \rho^* = \rho/\rho_0,\\
&D_1^* = D_1 T/L^2, && D_2^* = D_2 T/L^4, && r^* = rNT, &&\\
&\tau^* = \tau\rho_0 N(1+\nu)/E, && \mu_i^* = \mu_i(1+\nu)/ET && (i = 1, 2). &&
\end{aligned}\right\} \tag{13}$$

Depending on what time scale we are concerned with we can reduce the set of ten parameters by one. For example, if we choose T as the mitotic time, $1/(rN)$, then $r^* \equiv 1$. Similarly, we could choose T so that $\alpha^* \equiv 1$ or $\mu_i^* \equiv 1$ for $i = 1$ or 2. For simplicity in the analyses below we shall take $\lambda^* = 0$, but as will be clear, $\lambda^* \neq 0$ can easily be incorporated into the analysis.

In summary, the dimensionless field equations we shall discuss here are:

$$\partial n/\partial t = D_1\nabla^2 n - D_2\nabla^4 n - \alpha\nabla\cdot n\nabla\rho - \nabla\cdot(n\boldsymbol{u}_t) + rn(1-n) \tag{14a}$$

$$\nabla\cdot[\mu_1\boldsymbol{\varepsilon}_t + \mu_2\theta_t\boldsymbol{I} + \boldsymbol{\varepsilon} + \hat{\nu}\theta\boldsymbol{I} + \tau n(\rho + \beta\nabla^2 n)\boldsymbol{I}] = \rho s\boldsymbol{u} \tag{14b}$$

$$\partial\rho/\partial t + \nabla\cdot(\rho\boldsymbol{u}_t) = 0 \tag{14c}$$

where we have dropped the asterisks for notational convenience. Note that the dimensionless parameters, all of which are positive, fall into two groups: $\{\alpha, D_1, D_2, \tau, r, \beta\}$ associated with the cell properties, and $\{\mu_1, \mu_2, \hat{\nu}, s\}$ associated with the matrix properties.

3. Linear analysis and pattern formation potential

In order to model the spatial patterns that arise in embryonic development the model equations must give rise to spatial inhomogeneities. The model is nonlinear and there is little hope of finding useful analytical solutions; therefore, we are presently engaged in investigating their properties numerically. However, some insight into the model's behaviour can be gleaned by a linear analysis.

One of the applications of the theory is to the pattern formation process that accompanies the formation of skin organ primordia for feathers and scales. The initial cell aggregations which form these primordia differ in cell density from the surrounding tissue by fairly small amounts. Therefore, it is worthwhile to pursue the evolution of small perturbations of a uniform field, not only for the insight it provides for guiding numerical work, but also since the patterns themselves may involve solutions that fall within the linear regime.

The nontrivial uniform steady state of (14) is

$$n = \rho = 1, \qquad \boldsymbol{u} = \boldsymbol{0}. \tag{15}$$

The linear stability of this solution is found in the usual way, by seeking solutions of the linearized equations from (14a,b,c), namely

$$n_t - D_1\nabla^2 n + D_2\nabla^4 n + \alpha\nabla^2\rho + \theta_t + rn = 0, \tag{16}$$

$$\nabla\cdot[(\mu_1\boldsymbol{\varepsilon}_t + \mu_2\theta_t\boldsymbol{I}) + (\boldsymbol{\varepsilon} + \hat{\nu}\theta\boldsymbol{I}) + (\tau n + \tau\rho + \tau\beta\nabla^2\rho)\boldsymbol{I}] - s\boldsymbol{u} = \boldsymbol{0}, \tag{17}$$

and

$$\rho_t + \theta_t = 0, \tag{18}$$

where we have replaced n by $n-1$ and ρ by $\rho-1$ for algebraic convenience.

We seek solutions to the linearized equations by looking for solutions of the form

$$(n, \rho, \boldsymbol{u}) \propto e^{\sigma t + i\boldsymbol{k}\cdot\boldsymbol{r}} \tag{19}$$

where $\boldsymbol{k}$ is the wave vector and σ is the linear growth factor (not to be confused with the stress tensor). Substituting (19) into (16), (17), and (18) gives the dispersion relation $\sigma = \sigma(k^2)$ as solutions of the quadratic equation

$$\sigma[\mu k^2\sigma^2 + b(k^2)\sigma + c(k^2)] = 0 \tag{20a}$$

where the coefficients $b(k^2)$ and $c(k^2)$ are given by

$$\left.\begin{aligned} b(k^2) &= \mu D_2 k^6 + (\mu D_1 + \beta\tau)k^4 + (1 + \mu r - 2\tau)k^2 + s \\ c(k^2) &= \tau\beta D_2 k^8 + [\tau(\beta D_1 - D_2) + D_2]k^6 + \\ &\quad + [\tau(r\beta - D_1 - \alpha) + D_1 + sD_2]k^4 + (r + sD_1 - r\tau)k^2 + rs. \end{aligned}\right\} \tag{20b}$$

Here we have set $\mu \equiv \mu_1 + \mu_2$ and τ, μ, and s replace $\tau/(1+\hat{\nu})$, $\mu/(1+\hat{\nu})$, and $s/(1+\hat{\nu})$, respectively.

For any wave number k, if the solution to (20a), $\sigma(k^2)$, has its real part positive, then the linear solution (19) is unstable. From (20), if $k^2 = 0$, the spatially homogeneous case, $b > 0$ and $c > 0$ since all the parameters are positive. So

$\sigma = -c/b < 0$, and hence the solutions are stable. Thus for $\mathrm{Re}[\sigma(k^2)] > 0$ to exist we must have $k^2 \neq 0$ for at least some k. All the solutions (19) with these k are then linearly unstable, and grow exponentially with time. These unstable modes will evolve into finite-amplitude spatially structured solutions. Heuristically, it appears from the physics of the nonlinear system (14) that such exponentially growing solutions will not grow unboundedly. Numerical solution of the full nonlinear system bears this out. The linearly unstable solutions probably have some predictive value as to the qualitative character of the finite-amplitude solutions. This predictive ability of the linear analysis is usually limited to small wave numbers as is frequently the case with reaction–diffusion models (Murray, 1981*b*).

From the quadratic dispersion relation (20) the only way a solution with $\mathrm{Re}(\sigma) > 0$ can exist is if $b(k^2)$ or $c(k^2)$ is negative. Since the only negative terms involve the traction parameter, τ, a necessary condition for the model equations to admit spatially heterogeneous solutions is that $\tau > 0$. It is also clear from the physics of the mechanism that this has to be the case, since without traction, there is no aggregative term in the equations. So sufficient conditions for spatially structured solutions to exist are those which ensure that $b(k^2) < 0$ or $c(k^2) < 0$ for some $k^2 > 0$. The expressions for $b(k^2)$ and $c(k^2)$ in (20) determine the domains in parameter space where spatially inhomogeneous linearly unstable solutions exist. They also give the bifurcation surfaces in the parameter space; that is, the surfaces which separate homogeneous from inhomogeneous solutions. It is algebraically very complicated to determine these surfaces in general. In any case, because of the dimensionality of the system it would be of little conceptual help in understanding the basic features of the pattern formation process. It is more instructive to consider various special cases whereby we assume one or more of the various factors affecting cell motion and matrix deformation to be negligible. One result is to produce several simpler model mechanisms which are all capable of generating spatial patterns. Which mechanism is most appropriate for a given situation must be determined by the biology. We list here several interesting special cases of the model equations.

(i) $D_2 = \beta = 0$: no long range cell interactions.
$\alpha = 0$: no haptotaxis
$r = 0$: no cell division

From (14) the model reduces to

$$n_t = D_1 \nabla^2 n - \nabla \cdot (n \boldsymbol{u}_t), \tag{21a}$$

$$\nabla \cdot [(\mu_1 \boldsymbol{\varepsilon}_t + \mu_2 \theta_t \boldsymbol{I}) + (\varepsilon + \hat{\nu}\theta)\boldsymbol{I}] + \tau n \rho \boldsymbol{I}] = s\boldsymbol{u}, \tag{21b}$$

and

$$\rho_t + \nabla \cdot (\rho \boldsymbol{u}_t) = 0. \tag{21c}$$

From the dispersion relation (20)

$$\sigma(k^2) = [-b + (b^2 - 4\mu k^2 c)^{\frac{1}{2}}]/(2\mu k^2), \tag{22a}$$

$$b(k^2) = \mu D_1 k^4 + (1 - 2\tau)k^2 + s, \tag{22b}$$

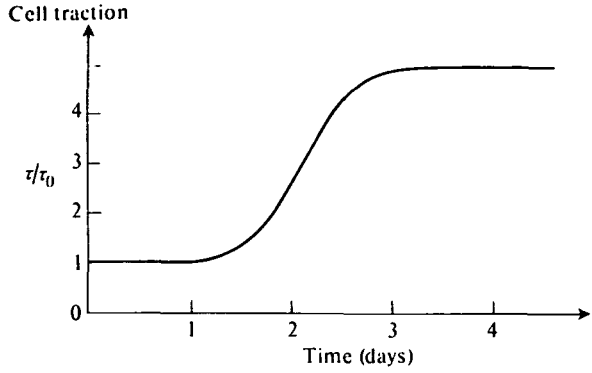

FIG. 1. Qualitative in vitro behaviour of the cell traction with time: τ_0 is a typical base value of the order of $10^{-2}\,\mathrm{N\,m^{-1}}$ per cell edge.

and

$$c(k^2) = D_1 k^2[k^2(1-\tau)+s] \tag{22c}$$

It is known that *in vitro* the traction generated by a cell can increase with time qualitatively as shown in Fig. 1. Therefore, we take τ as the bifurcation parameter, so that as τ increases the uniform steady state bifurcates to a spatially unstable state at $\tau = \tau_c$ (if $\tau_c < 1$), which is the value of τ where the minimum of $b(k^2)$ is zero. From (20), the critical values of τ and k^2 are:

$$\tau_c = \tfrac{1}{2} + (\mu s D_1)^{\frac{1}{2}} \tag{23a}$$

and

$$k_c = \left(\frac{s}{D_1 \mu}\right)^{\frac{1}{4}} \tag{23b}$$

The dispersion relation is illustrated in Fig. 2a.

An even simpler model which still exhibits spatial structure has $D_1 = 0$. Here, from (22), $\sigma > 0$ for all wave numbers $k^2 > s/(2\tau - 1)$ if $\tau > \tfrac{1}{2}$. The corresponding dispersion relation is illustrated in Fig. 2b. However, in this case there is an

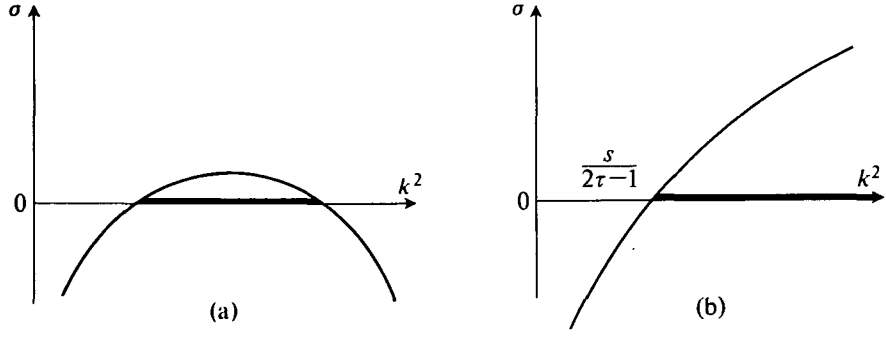

FIG. 2. Dispersion relation $\sigma = \sigma(k^2)$ for two particularly simple model systems (a) equations (21), (b) equations (21) with $D_1 = 0$. Unstable wave numbers are denoted by a heavy line.

infinite range of unstable wave numbers which suggests that the ultimate spatial structure depends intimately on the initial conditions.

(ii) $D_1 = D_2 = 0$: no cell diffusion,

$\alpha = 0$: no haptotaxis,

$\mu_1 = \mu_2 = 0$: no viscoelastic effects in the matrix equation.

Here the model (14) reduces to a remarkably simple system which, in one spatial dimension, is

$$n_t + (nu_t)_x - rn(1-n) = 0, \tag{24a}$$

$$\frac{\partial}{\partial x}[u_x + \tau n(\rho + \beta\rho_{xx})] - \rho s u = 0, \tag{24b}$$

and

$$\rho_t + (\rho u_t)_x = 0. \tag{24c}$$

The dispersion relation in this case has, from (20),

$$b = \tau\beta k^4 + (1-2\tau)k^2 + s$$

and

$$c = \tau\beta r k^4 + r(1-\tau)k^2 + rs.$$

The $\sigma(k^2)$ is plotted in Fig. 3. Note that the range of unstable wave numbers is finite, and that there are two bifurcation values for the traction parameter, τ. This example illustrates the remarkable richness of pattern formation potentialities which even simple cases of (14) can exhibit. Murray & Oster (1984) discuss a

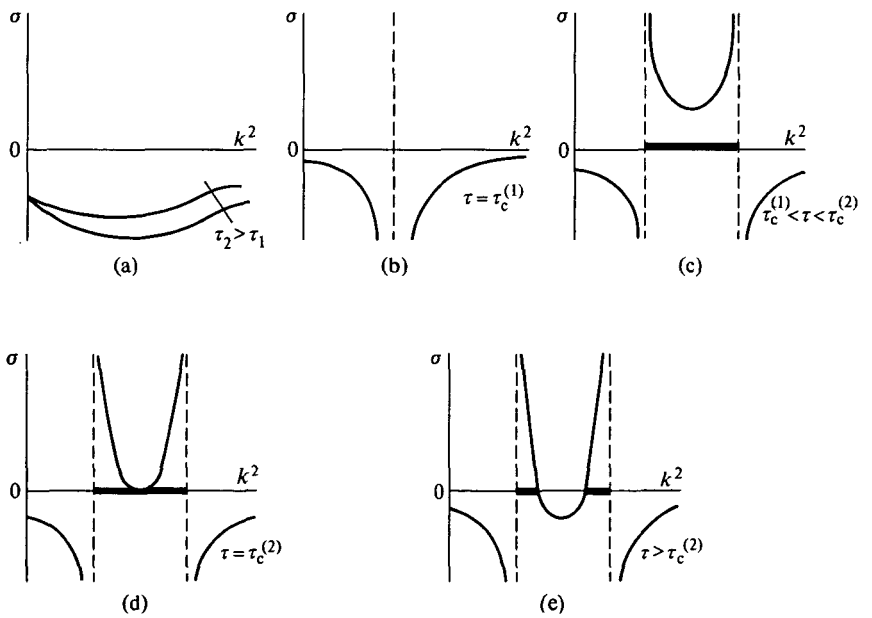

FIG. 3. Illustrative dispersion relations $\sigma = \sigma(k^2)$ for the model system (24): unstable wave numbers are denoted by a heavy line.

variety of special cases of (14) which exhibit a finite range of unstable modes, and others which have an infinite range of unstable wavenumbers.

From the viewpoint of biological applications, two- and three-dimensional patterns are of great interest. With the experience gained from reaction–diffusion spatial patterns we expect that the simulated patterns will reflect the qualitative features of the linear analyses. This motivates us to look for possible symmetries in the solutions. We do this by taking the divergence of (17) to yield the system

$$n_t + D_2\nabla^4 n - D_1\nabla^2 n + \alpha\nabla^2\rho + \theta_t + rn = 0, \tag{25a}$$

$$\nabla^2[\theta_t + (1+\hat{v})\theta + \tau\rho + \tau\beta\nabla^2\rho] - s\theta = 0, \tag{25b}$$

and

$$\rho_t + \theta_t = 0. \tag{25c}$$

Relevant solutions to this set of equations are not trivial to determine. However, we can look for solutions which are spatially periodic:

$$\chi(\boldsymbol{r} + m\boldsymbol{\omega}_1 + l\boldsymbol{\omega}_2) = \chi(\boldsymbol{r}) \tag{26}$$

where $\chi = (n, \boldsymbol{u}, \rho)$, m and l are integers and $\boldsymbol{\omega}_1$, $\boldsymbol{\omega}_2$ are independent vectors. Such solutions tesselate the plane. From the linear system (25), the class of periodic solutions include at least the eigenfunctions of

$$\nabla^2\psi + k^2\psi = 0, \qquad \hat{\boldsymbol{n}}\cdot\nabla\psi = 0, \tag{27}$$

where $\hat{\boldsymbol{n}}$ is the unit normal vector on the domain boundary. With these boundary conditions the solutions of (25) are periodic. Regular plane periodic tesselation has the basic symmetry groups of the square, rhombus, and hexagon solutions. For the hexagonal solutions:

(hexagon)
$$\psi(r, \phi) = \tfrac{1}{3}\{\cos[kr\sin(\phi + \pi/6)] + \cos[kr\sin(\phi - \pi/6)] + \cos[kr\sin(\phi - \pi/2)]\},$$

and hence
$$\psi(r, \phi) = \psi(r, \phi + \pi/3) = H\psi(r, \phi) \tag{28}$$

which shows that the solution is invariant under the hexagonal rotation H. Typical hexagonal solutions are illustrated in Fig. 4b. The hexagonal pattern is of particular biological significance, as we discuss below.

Solutions with square rotational invariance have the property

(square)
$$\psi(x, y) = \tfrac{1}{2}[\cos kx + \cos ky]$$

and hence
$$\psi(r, \phi) = \tfrac{1}{2}[\cos(kr\cos\phi) + \cos(kr\sin\phi)] \tag{29}$$

and
$$\psi(r, \phi) = \psi(r, \phi + \pi/2) = S\psi(r, \phi)$$

where S is the square rotation. This is illustrated in Fig. 4a.

The rhombic solution, illustrated in Fig. 4c, with δ the rhombic angle, is

(rhombus)
$$\psi(r, \phi) = \tfrac{1}{2}\{\cos(kr\cos\phi) + \cos[k\cos(\phi - \delta)]\}$$

and hence
$$\phi(r, \phi; \delta) = \psi(r, \phi + \pi; \delta) = R\psi(r, \phi; \delta) \tag{30}$$

where R is the rhombic rotation.

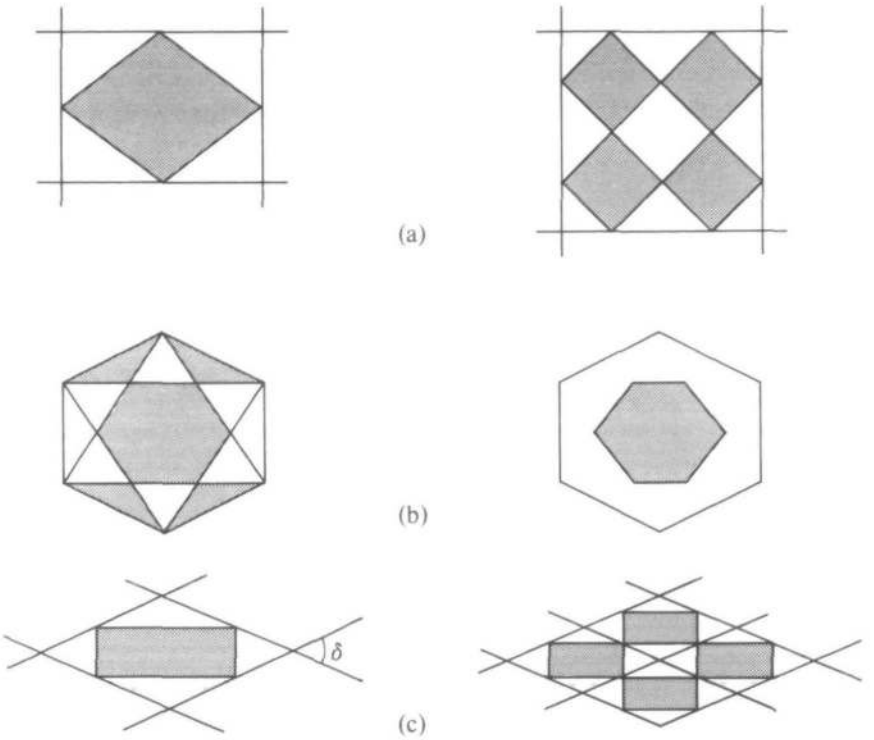

FIG. 4. Plane periodic pattern solutions of equation (27): (a) square, (b) hexagonal, (c) rhombic.

Perhaps it should be mentioned here that the spectrum of spatial patterns possible with the mechanism (14) is much greater than that possible with even a three-component reaction–diffusion system. For example, Penrose (1979) has suggested that certain singularities observed in dermal ridges cannot be generated by a vector field model, but can arise from a symmetric tensor field, such as stress or strain. The analytical and numerical study of the cell traction model (14) has only just begun.

4. Biological applications of the model

Generation of regular patterns of cell aggregation occurs in many situations in early embryogenesis. We have already mentioned the cases of feather and scale primordia and the condensations of precartilage cells in bone formation. Here we discuss both of these in somewhat more detail and point out some other areas where the model may find some relevance.

4.1 *Periodic Patterns of Feather Germs*

Feather primordia first appear as local thickenings of the epidermis, called placodes, underlain by local aggregations of dermal cells, called papillae. Although it is not yet settled whether the placodes or the papillae appear first,

transplant experiments indicate that the spatial pattern is dictated by the dermis (Sengel, 1976). Recent work by Davidson (1983) demonstrates that the primordia appear sequentially: a central column of dermal cells forms which subsequently breaks up into a row of papillae in an anterior-posterior sequence. Then lateral rows of papillae form sequentially from anterior to posterior between the initial condensations.

These observations indicate that it is appropriate to model the initial row of papillae by a one-dimensional column of cells and look for the conditions for spatial instability. This is stage 1 in Fig. 5. The critical wavelength, $1/k_c$, at which the pattern appears should give an estimate of the spacing of the condensations. Indeed, the situation wherein the uniform solution bifurcates to a spatially inhomogeneous one may not be relevant: the sequential appearance of the papillae that Davidson (1983) observes may well be generated by a kinematic parameter wave which sweeps down the column. There is some indication that this wave is related to the age of the tissue; in this case we can sequentially raise, say, the traction parameter, τ, down the column and observe the pattern.

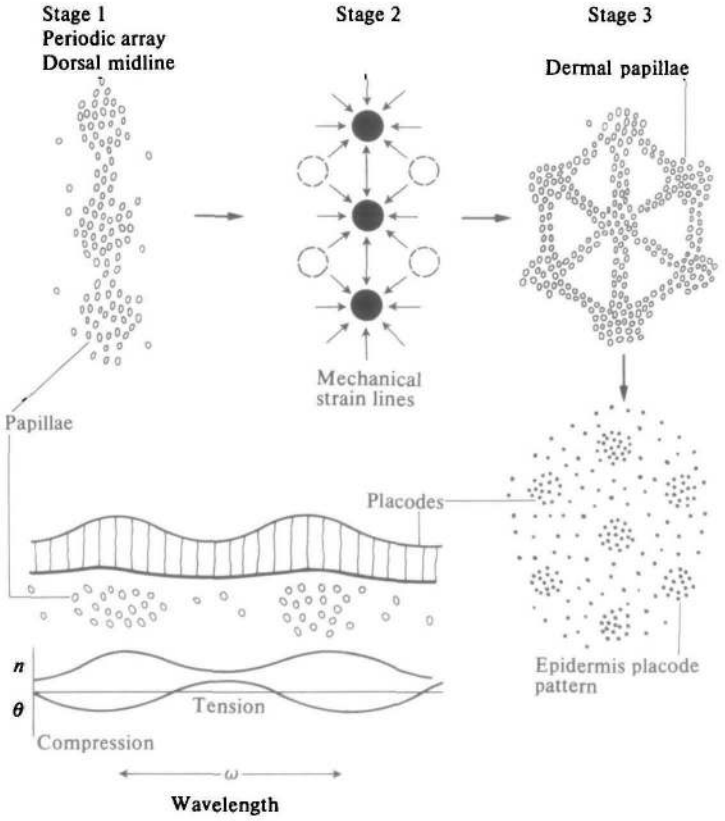

FIG. 5. Model morphogenesis of feather/scale primordia. The papillae wave length is a function of the ECM parameters (μ, ρ_0, E, ν, s) and the cell parameters (α, τ, β, D_1, D_2, r, N). Epidermis mitosis is enhanced and inhibited by the underlying tension and compression respectively.

Simulations show that the spacing obtained in this sequential fashion is nearly the same as that obtained from a homogeneous bifurcation. This is not expected to be the case in two or three dimensions.

The pattern of matrix strains set up by the initial row of papillae produces minima in a staggered row lateral to the central row. This clearly biases the formation of the secondary condensations to these locations (stage 2 of Fig. 5), since the effects of cell traction are less dominated by the existing rows. Thus we can see how hexagonal patterns arise, as shown in stage 3 of Fig. 5. Numerical simulations, to be presented elsewhere, bear out this scenario.

One of the most useful aspects of forming dimensionless equivalents of the model equations is that it is possible to assess how different physical effects trade off against one another. For example, from (13) we see that in model (21), say, the effect of reducing the cell traction, τ, has the same effect as increasing the cell density or decreasing the elastic modules, E. Thus an important caveat in interpreting experimental manipulations is that quite different cell or matrix alterations can produce compensating, and therefore equivalent, results (see Oster, Murray, & Harris, 1983).

4.2 *Cartilage Condensations in Limb Morphogenesis*

In developing limb buds aggregations of chondrocytes presage the cartilage patterns which later ossify into bones. The chondrocytes are mesenchymal cells such as we have been considering, and so the possibility is attractive that the same sequential pattern formation mechanism discussed for the feather germs applies to this situation. This situation is discussed in detail in Oster *et al.* (1983), and the scenario is illustrated in Fig. 6. The argument is, briefly, as follows.

As the limb bud grows, the domain is only slightly ellipsoidal in cross-section. Thus the first bifurcation produces a single central aggregation of cells. As these cells condense, the stress generated is directed radially inwards toward the limb axis. This radial stress deforms the cross-section, making it even more elliptical. The changing geometry, in turn, induces a secondary bifurcation in a fashion similar to that discussed in a reaction–diffusion model by Murray (1981*a*). Thus

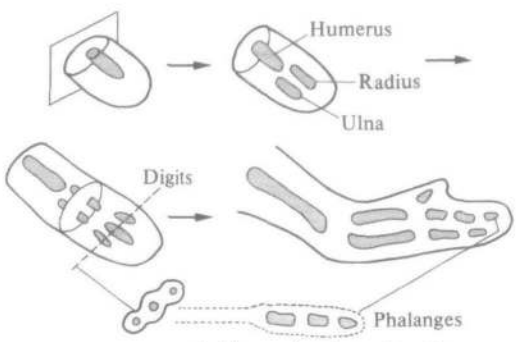

FIG. 6. Bifurcation scenario for cartilage formation in the developing chick limb.

the condensation of cells influences the shape of the domain, which in turn controls the sequence of bifurcations. This sequence of bifurcations need not be generated completely by a changing geometry; as the above discussion concerning dimensionless ratios shows, it can result from a combination of variations in other parameters.

Recent experimental evidence from amphibians suggests that the osmotic properties of the ECM may be important (P. Alberch, 1983; personal communication). A principle component of the ECM is hyaluronate which, under physiological conditions, exists in a highly swollen osmotic state. Just at the time of condensation the chondrocytes commence to secrete hyaluronidase, an enzyme which degrades the hyaluronate. This probably leads to an osmotic collapse (syneresis) of the matrix gel, which brings the cells close enough together to initiate active contractions. Cell motility may only be a secondary effect under this scenario. This situation requires only a small modification of the matrix mechanical equation to include osmotic effects. In particular, we must add a term to the stress tensor which models the swelling pressure, π_s, of the ECM and its control by the hyaluronate. We shall discuss this important modification in a subsequent publication.

4.3 *Animal Coat Patterns*

In a series of papers Murray (1979, 1981*a*,*b*) showed that many of the patterns observed on mammalian coats could be generated with a morphogen based reaction–diffusion model. The patterns thus generated were considered the prepatterns for the melanoblast cells—the precursors of the pigment forming melanocytes. The evidence presented for such a theory was based on observational comparisons and on certain developmental constraints which were dictated by the geometry and the scale of the animal's surface at the time the prepattern was laid down.

However, the melanoblast cells which form the pattern migrate from the neural crest early in development. Since our model here deals directly with such migratory cells, it is perhaps more directly applicable to the patterns found on mammalian coats. Indeed, in view of the above discussion as to the relative richness of patterns which can be obtained from the cell traction model as compared with morphogen models, it is clear that we can obtain not only similar patterns to those from the reaction–diffusion mechanism, but others which the morphogen model cannot produce. Since the partial differential equations (14) are also domain- and boundary-dependent in the same way as the morphogen model, the same kind of developmental constraints found by Murray (1979, 1981*a*,*b*) apply to the mechanical model. A more detailed description of this problem will be presented elsewhere.

4.4 *Wound Healing*

The disfiguring scars produced from wounds, particularly those associated with burns, result principally from 'wound contracture'—deformations of the tissue

resulting from the traction forces generated by the dermal cells migrating into the wound region. The shape of the boundary is known to affect the amount of scarring. The cell traction model appears to offer the possibility of designing surgically induced wound perimeter geometries which could minimize contracture scarring. This is a free-boundary-value problem of great complexity, and even numerical simulation will not be easy. However, the possible benefits accruing from such a program would unquestionably be worth some effort.

4.5 *Rejection of Artificial Joints*

One of the problems associated with artificial hip joints is that the cement for fixing them in place inside the femur frequently does not form a good bond with the living tissue. The concepts used in setting up the mechanism discussed here have suggested that a method of obtaining a better bond is to use an adhesive which is sufficiently porous to allow migration of cells into it. Experimental work on this is currently in progress (Y. K. Liu, 1984; personal communication).

5. A continuum model for epidermal sheets

The second major tissue system that constitutes the early embryo is the epithelia. Here the cells which, unlike the mesenchyme, are not actively motile but are arranged in layers, or sheets. These sheets bend and deform during morphogenesis. In most cases, epithelial morphogenesis evolves due to the shape changes of the individual cells and cells tend to maintain contact with their nearest neighbours (there are important exceptions to this, but we shall not be concerned with those here). Moreover, many morphogenetic processes, including the skin primordia, depend on the chemical and mechanical interaction between the mesenchymal cells and the epithelial cells upon which they crawl. Indeed, tissue interactions are one of the major phenomena associated with the developing embryo (Wessells, 1977).

Odell *et al.* (1981) proposed a finite-element model for epithelial sheets. This model was based on the cytological observation that many epithelia have an apical band of contractile microfilaments whose contractions can deform the cell. They demonstrated that many morphogenetic movements of epithelial sheets could be understood, at least in part, as resulting from the mechanical interactions between the constituent cells. Their model was based on the assumption that the microfilament bundle which controls the cell shape could be triggered to contract by an internal release of calcium (Odell *et al.*, 1981; Oster & Odell, 1984) or by mechanically stretching the cell (Odell *et al.*, 1981). In this section we generalize the discrete model of Odell *et al.* to a continuum model, which has the advantage of allowing some analytical treatment, as well as enhancing our understanding of the mechanics of cytogels.

5.1 *Some Biological Facts About Cytogel*

The cellular cytoplasm near the periphery of the cell consists largely of a viscoelastic gel: a network of macromolecular fibres composed mostly of actin and

myosin, the same molecules involved in muscle contraction. This cytogel is a dynamic structure: the cell can regulate the degree of assembly and crosslinking of the fibres as well as their propensity to contract actively. By regulating the sol–gel equilibrium of the gel and its state of contraction, the cell can carry out an astounding variety of motile phenomena and shape changes. We shall not endeavour to model all of the complexity of this system, but rather focus on a few physical properties which are sufficient to understand the morphogenesis of epithelial sheets. In particular, we shall not model explicitly the sol–gel transitions, but incorporate the equivalent mechanical effect into the gel constitutive relation.

Chemical control of contractility is largely attributable to the local concentration of free calcium in the cytogel. Calcium regulates the activity of the solation and gelation factors as well as the activity of the actomyosin contractile machinery. At low calcium levels the gel is highly crosslinked and stable. As calcium concentrations rise to the micromolar level the gel commences to solate partially, and to contract actively. If the calcium level rises too high, however, the gel becomes so solated that it cannot support any stress. Thus there is a 'window' of calcium concentration which is optimal for contractile activity.

5.2 *A Mechanical Model for Cytogel Contractility*

It turns out that in many embryological processes the reticulation of cytogel into cells is not essential for carrying out the process; for example, mitotic inhibitors which prevent cell division do not inhibit such phenomena as pseudogastrulation in amphibian eggs. Moreover, organisms such as *Physarum* are able to carry out major morphogenetic movements without benefit of cell partitions (Oster & Odell, 1984). Therefore, we shall model an epithelial sheet as a continuum of cytogel; this means that we shall ignore the membrane that delimits each cell.

As for the mesenchymal model, inertial forces are negligible, and the mechanical equation of motion can be written as

$$\nabla \cdot \boldsymbol{\sigma} + \rho \boldsymbol{F} = \boldsymbol{0} \tag{31}$$

where $\boldsymbol{\sigma}$ is the stress tensor, $\boldsymbol{F}$, the body forces and ρ the cytogel density. As before, we shall assume that the viscoelastic stress, $\boldsymbol{\sigma}$, can be decomposed into a linear viscous term, $\boldsymbol{\sigma}_V$, and an elastic stress, $\boldsymbol{\sigma}_E$:

$$\begin{aligned} \boldsymbol{\sigma} &= \boldsymbol{\sigma}_V + \boldsymbol{\sigma}_E \\ &= (\mu_1 \boldsymbol{\varepsilon}_t + \mu_2 \theta_t \boldsymbol{I}) + [E/(1+\nu)](\boldsymbol{\varepsilon} + \hat{\nu}\theta \boldsymbol{I}) + \tau \boldsymbol{I} \end{aligned} \tag{32}$$

τ is the contribution of the active traction to the elastic stress, and the coefficients μ_i, E, and ν have the same significance as in the mesenchymal model; in this model, however, the parameters will not be constant. The relationship between the two models is this: the mesenchymal model viewed the cell–matrix material as an elastic continuum in which were embedded motile contractile units: the cells. Here, the elastic continuum also has contractile units: the actomyosin crossbridges. However, since we shall not deal with the solation of the gel

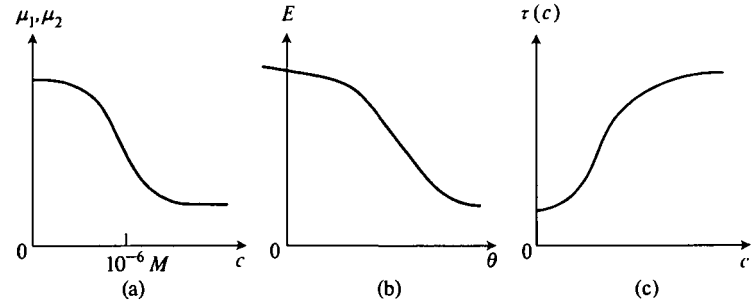

FIG. 7.

network, we do not have to account for the motion of the contractile units apart from the deformation of the gel itself. In this model the role of the cells is replaced by the chemical trigger for contraction, free calcium ion, which we denote by $c(\boldsymbol{r}, t)$. We model the constitutive parameters μ, E, and τ as follows.

(i) Viscosity. The severing of the gel network by the calcium activated solation enzymes results in a precipitous drop in the apparent viscosity. Indeed, this has many of the aspects of a phase transition, and so we model $\mu_i(c)$ by the sigmoidal curve shown in Fig. 7a.

(ii) Elasticity. A characteristic property of actomyosin fibrils is that as they shorten, the amount of overlap of the actin fibres increases, and also the number of active crossbridges. Therefore, as a fibre contracts it grows stronger. Moreover, when a fibrous material is strained, the fibres tend to align and the apparent elasticity increases. To model this latter effect we would have to abandon the isotropic model, and so we content ourselves with modelling these nonlinear effects by assuming that E decreases with dilatation, θ, as shown in Fig. 7b.

(iii) Active Traction. Once the actomyosin machinery has been triggered to contract, the fibres commence to generate contractile stresses. Once again, the onset of contraction is rather sudden, in the micromolar range. Therefore, we model the active stress contribution, τ, by the sigmoidal curve shown in Fig. 7c (Oster & Odell, 1984). Alternatively, we can view the traction stress, $-\tau(c)$ as the new rest configuration to which the fibres attempt to contract (Odell *et al.*, 1984). Any displacement of the epithelium is resisted by its attachment to the basal lamina in the form of restraining tethers. We model this force by taking $F = \rho s \boldsymbol{u}$ where s is a parameter reflecting the strength of the attachment.

With these modifications, the mechanical equation of motion for the cytogel takes the form

$$\nabla \cdot \left(\mu_1 \boldsymbol{\varepsilon}_t + \mu_2 \theta_t \boldsymbol{I} + \frac{E(\theta)}{1+\nu} [\boldsymbol{\varepsilon} + \hat{\nu} \theta \boldsymbol{I} + \tau(c) \boldsymbol{I}] \right) - \rho s \boldsymbol{u} = \boldsymbol{0}. \tag{33}$$

5.3 *Conservation Equation for Calcium*

The equation governing the release and diffusion of calcium, $c(\boldsymbol{r}, t)$, has the form

$$\frac{\partial c}{\partial t} = D \nabla^2 c + R(c, \boldsymbol{\varepsilon}) \tag{34}$$

where D is the diffusion coefficient for calcium and $R(c, \varepsilon)$ is the calcium kinetics of release and resequestration. The kinetics has three contributions.

Calcium is sequestered in membranous vesicles dispersed throughout the cytogel. These vesicles have the property of calcium-stimulated calcium release (see Oster & Odell, 1984); that is, if the level of free calcium outside the vesicles exceeds a certain threshold, it induces the membrane channels to open and the vesicles release their internal stores of calcium. How this autocatalytic release mechanism works is not yet known; however, we can model it phenomenologically by a threshold kinetics similar to the FitzHugh–Nagumo model for nerve excitation. That is, we assume that the release kinetics is governed by a sigmoidal (autocatalytic) curve, and that resequestration takes place by a first-order process. A typical analytical form for such kinetics is

$$R(c) = \alpha c^2/(1+\beta c^2) - \delta c \tag{35}$$

where α, β, and δ are positive constants. The form of $R(c)$ is S-shaped, as shown in Fig. 8a, so that there are two stable equilibria, at 0 and c_3, separated by an unstable equilibrium at c_2.

The autocatalytic release mechanism can also be triggered by straining the cytogel, a phenomenon called 'stretch activation'. This probably is caused by depolarizing the vesicle membrane by mechanical deformation. Whatever the mechanism, we can add the effect to the release kinetics by introducing a leak term, $\gamma\theta$, into equation (35), so that the release kinetics has the form

$$R(c, \varepsilon) = \alpha c^2/(1+\beta c^2) - \delta c + \gamma\theta \tag{36}$$

where the positive parameter, γ, is the release rate per unit strain. The effect of strain on the release kinetics is shown in Fig. 9b: increasing θ raises the curve until the leftmost equilibrium, c_1, disappears, and the system moves to the equilibrium at c_3. We emphasize that the formula (36) is illustrative—only the qualitative features of $R(c, \varepsilon)$ are important to the functioning of the model. Murray (1981) used a similar biochemical 'switch' mechanism to model the formation of wing patterns in butterflies.

Thus the equation of motion for the free calcium concentration is

$$\frac{\partial c}{\partial t} = D\nabla^2 c + \frac{\alpha c^2}{1+\beta c^2} - \delta c + \gamma\theta \tag{37}$$

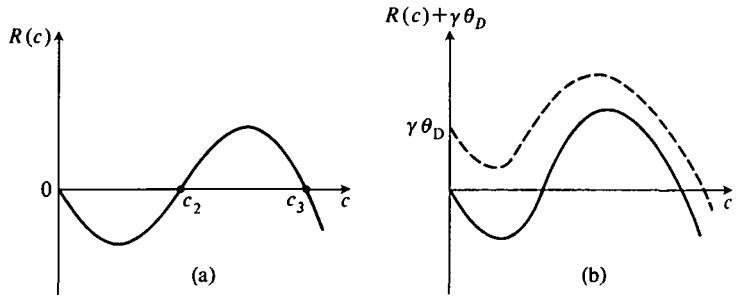

FIG. 8.

The model cytogel consists of the mechanical equation (33) and the coupled chemical equation (37). Workers familiar with the theory of thermoelasticity will notice a striking similarity in the form of the equations.

6. Analysis of the model equations

Proceeding as we did in the mesenchymal model, we form dimensionless equivalents of the equations by means of the following substitutions.

$$\left.\begin{array}{c} \boldsymbol{r}^* = \boldsymbol{r}/L, \qquad t^* = \gamma t/c_3, \qquad c^* = c/c_3, \qquad \boldsymbol{u}^* = \boldsymbol{u}/L, \\ \theta^* = \theta, \qquad s^* = \rho s L^2(1+\nu)/E(0), \qquad \mu_i^* = \gamma\mu_i(1+\nu)/[c_3E(0)] \quad (i=1,2), \\ R^*(c^*) = R(c)/\gamma, \qquad D^* = Dc_3/(L^2\gamma), \qquad \tau^*(c^*) = \tau(c), \\ E^*(\theta^*) = (1+\nu)E(\theta)/E(0) \end{array}\right\} \tag{38}$$

where L is a characteristic length scale. Substituting these into the field equations (33) and (37), and omitting the asterisks for notational simplicity, we have the dimensionless equations for a cytogel continuum:

$$\nabla\cdot\{\mu_1\boldsymbol{\varepsilon}_t + \mu_2\theta_t\boldsymbol{I} + E(\theta)[\boldsymbol{\varepsilon} + \hat{\nu}\theta\boldsymbol{I} + \tau(c)\boldsymbol{I}]\} - s\boldsymbol{u} = \boldsymbol{0} \tag{39a}$$

$$\partial c/\partial t = D\nabla^2 c + \alpha c^2/(1+\beta c^2) - \delta c + \gamma\theta \tag{39b}$$

The boundary conditions for (39) depend on the problem under consideration. Typical boundary conditions are periodic or stress-free boundaries for the mechanical equation, and impermeable boundaries for the chemistry.

6.1 *Linear Stability Analysis*

Equations (39) have spatially uniform steady-state solutions

$$\boldsymbol{u} = \theta = \boldsymbol{0}, \qquad c = c_i \quad (i = 1, 2, 3) \tag{40}$$

We carry out a linear stability analysis exactly as in Section 3, by seeking solutions of the form $\exp(\sigma t + i\boldsymbol{k}\cdot\boldsymbol{r})$. The dispersion relation so obtained is

$$(\sigma\mu_1 k^2 + k^2 + 2s)[\mu k^2\sigma^2 + b(k^2)\sigma + d(k^2)] = 0 \tag{41a}$$

where

$$b(k^2) = \mu D k^4 + (1 + \hat{\nu} - \mu R_i' + E'\tau_i)k^2 + s \tag{41b}$$

and

$$d(k^2) = D(1+\hat{\nu}+E'\tau_i)k^4 + [sD + \tau_i'\gamma - R_i'(1+\hat{\nu}+E'\tau_i)]k^2 - R_i's. \tag{41c}$$

Here we have employed the notations:

$$\mu \equiv \mu_1 + \mu_2, \qquad R_i' \equiv \left[\frac{dR(c)}{dc}\right]_{c_i}, \quad \text{and} \quad \tau_i \equiv \left[\frac{d\tau(c)}{dc}\right]_{c_i}.$$

From Figs. 8 and 9, we have

$$E' < 0, \qquad \tau_i > 0, \qquad \tau_i' > 0, \qquad R_2' > 0, \quad \text{and} \quad R_i' < 0 \quad (i = 1, 3). \tag{42}$$

So, for $i=1,3$ we have $b(k^2)>0$ and $d(k^2)>0$, which shows that the three solutions for $\sigma(k^2)$ in (41) have $\mathrm{Re}\,(\sigma)<0$, and hence that the steady states

$$\boldsymbol{u}=\boldsymbol{0}, \qquad c=c_1 \quad \text{and} \quad \boldsymbol{u}=\boldsymbol{0}, \qquad c=c_3$$

are linearly stable. The steady state at $\boldsymbol{u}=\boldsymbol{0}$, $c=c_2$ is unstable, even in the absence of any spatial effects; that is, $k^2\equiv 0$, since $b(0)=s>0$ $d(0)=-R_2'\mathrm{s}<0$ and hence $\sigma(0)>0$ from (41). In the situation where $k^2\neq 0$ there is a critical wave number, k_c, where $d(k^2)>0$ if $k>k_c$, which implies stability.

From the linear analysis it appears that no spatial structure can be generated without a contribution from the dermis; that is, $\theta(\boldsymbol{r})\neq 0$. However, suppose that the dermis exerts a constant contraction: $\theta_D=\text{constant}>0$, which we add to the right-hand side of (39). Then the steady states are solutions of

$$R(c)+\theta_D=0, \qquad \boldsymbol{u}=\boldsymbol{0}.$$

The qualitative relationships can be seen from Fig. 8b: the effect of θ_D is the same as that of increasing the stretch activation term, $\gamma\theta$. If θ_D is strong enough, the curve is raised above the firing level, and the epithelium will be triggered to contract. Thus it is clear that a nonuniform dermal cell distribution can trigger the epithelial sheet to form placodes. That is, our analysis predicts that the dermal papillae may precede the epidermal placodes. Of course, the epidermis could also be triggered to disrupt its uniform state by an influx of calcium (or some signal, such as a depolarization wave or trigger chemical that stimulated the calcium cascade). However, it is an attractive feature of the model that it may depend on tissue interactions between the dermis and epidermis to initiate pattern formation.

6.2 *Travelling Wave Solutions*

One of the most interesting features of the model of cytogel model of Odell and Oster (1984) is its ability to propagate contraction waves. Intuitively, we expect the continuum model we have constructed here to exhibit similar behaviour. As a first step in finding such travelling wave solutions we consider the one-dimensional problem. In this case, $\varepsilon=\theta=u_x$, and the model equations become

$$\mu u_{xxt}+\frac{\partial}{\partial x}\{E(u_x)[(1+\hat{\nu})u_x+\tau(c)]\}-su=0 \tag{43a}$$

and

$$c_t-Dc_{xx}-\gamma u_x-R(c)=0, \tag{43b}$$

where $\mu\equiv\mu_1+\mu_2$. We seek travelling wave solutions of the form

$$u(x,t)=U(z), \qquad c(x,t)=C(z), \quad \text{and} \quad z=x+Vt$$

Upon substitution into [43] we find that $U(z)$ and $C(z)$ satisfy

$$\mu V\frac{\mathrm{d}^3U}{\mathrm{d}z^3}+\frac{\mathrm{d}}{\mathrm{d}z}\left[E\frac{\mathrm{d}U}{\mathrm{d}z}\left((1+\hat{\nu})\frac{\mathrm{d}U}{\mathrm{d}z}+\tau(C)\right)\right]-sU=0$$

and

$$D\frac{d^2C}{\mathrm{d}z^2}+\gamma\frac{\mathrm{d}U}{\mathrm{d}z}-V\frac{\mathrm{d}C}{\mathrm{d}z}+R(C)=0.$$

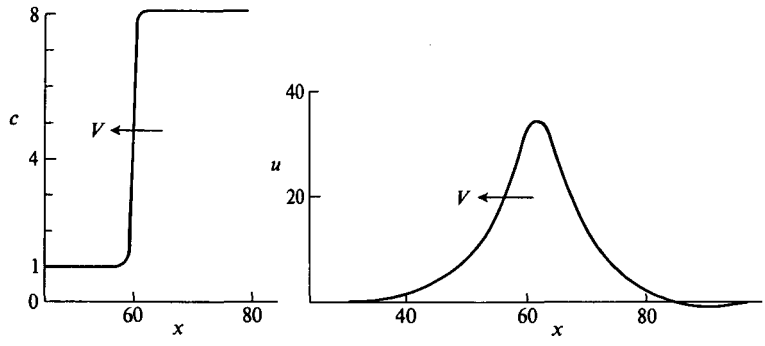

FIG. 9. Travelling wave solution for equations (43) with (a) the calcium concentration wave and (b) the displacement wave. Parameter values: $\gamma = 10{\cdot}0$, $\mu = 1{\cdot}0$, $D = 10{\cdot}0$, $s = 0{\cdot}1$, $E(1+\hat{\nu}) = 1{\cdot}5$ $R(c) = (1-c)(c-2)(c-8)$,

$$\tau(c) = \begin{cases} 0{\cdot}75 & c < 1{\cdot}5 \\ 0{\cdot}25 + (c-2{\cdot}5)(2c^2 - 7c + 5) & 1{\cdot}5 \leqslant c \leqslant 2{\cdot}5 \\ 0{\cdot}25 & 2{\cdot}5 < c \end{cases}$$

This is a fifth order system whose phase-space analysis is quite difficult. However, various approximations can be made. For example, for the propagation of contraction waves the dependence of E on ε is not crucial. However, in order to reduce the dimensionality of the phase space either, or both, of D and μ must be taken as zero. Unfortunately, this is probably a bad assumption, for both are not negligible in the biological situation. Thus analytical investigation of the equations for travelling waves must remain an open question. However, numerical simulations can be done, and Fig. 9 shows one example of the wave profiles obtained with the boundary conditions $U(\pm\infty)=0$, $C(-\infty)=c_1$, and $C(\infty)=c_3$, the nonzero stable steady states.

The wave speed is computed to be $v = (L\gamma/c_3)V$, where c_3 is the largest root of $R(c) = 0$ and V is the dimensionless wave speed. If we use the elastic constant s to obtain a length scale, L, the velocity is

$$v = \left(\frac{E(0)}{s(1+\nu)}\right)^{\frac{1}{2}} \frac{V}{c_3},$$

from which we see that the speed of the wave varies inversely with the strength of the forces attaching the sheet to the substratum. The qualitative dependence of the propagation speed on the other parameters is not always so clear, since they appear in dimensionless groupings. For example, choosing L as the diffusion length

$$v = [Dc_3/\gamma]^{\frac{1}{2}} V.$$

Numerical studies of the one-dimensional system are currently underway.

7. Biological applications

(1) In the marine organism *Acetabularia* the head regenerates after amputation. During regeneration a variety of events take place, one of which is the

appearance of a regular pattern of hair primordia around the stem. It is known that calcium ions play a crucial role in the process (Goodwin, Murray, & Baldwin, 1984). For example, if too little free calcium is present in the surrounding medium no pattern evolves. On the other hand, if too much calcium is present pattern formation is also inhibited. Associated with this regular pattern are wrinkles in the stem near the tip where the pattern appears. The model cytogel we have discussed can possibly produce periodic arrays of thickenings which resemble the hair primordia; investigation of this system is currently underway.

(2) Hair cells are the sensory transducers in the inner ear which convert acoustical pressure waves into nerve impulses. These cells are covered with rod-like protuberances called stereocilia which are packed in regular hexagonal arrays (Hudspeth, 1983). Oster, Murray, & Odell (1984) have shown that a viscoelastic model closely related to the above model can produce such hexagonal arrays.

(3) By including osmotic pressure effects and the possibility of network depolymerization, Oster & Perelson (1984) have constructed a cytogel model for lamellipodia, the motile appendage of crawling cells. The model is able to account for most of the observed properties of cell motion, including contact inhibition, traction and strain guidance, chemotaxis and galvanotaxis.

8. Conclusions

The development of pattern and form in embryogenesis is immensely complex and little of it is yet understood in terms of physical mechanisms, despite a huge body of experimental observation. There is no doubt that chemical and mechanical processes are involved, but elucidating just how they conspire to bring about morphogenetic movements has proved elusive. We have presented here two models which show how the interaction of mechanical forces with quite simple chemistry can generate patterns which bear a striking resemblance to biological structures.

The models presented here have a different flavour from reaction–diffusion models: in the latter a chemical (morphogen) field sets up a prepattern which is *then* read out and interpreted by the cells which then execute some hypothesized program of shape change and differentiation. In the mechanochemical models above, pattern formation does not precede morphogenesis; rather they evolve simultaneously and in synchrony.

Another distinction between the mechanochemical approach and reaction–diffusion models addresses the issue of experimental accessibility. It has been repeatedly emphasized in the morphogenesis literature that 'morphogens', like hormones, may act in concentrations so small as to defy detection. Indeed, analysis of morphogen models show that since activator and inhibitor substances mutually affect one another's production, it may be quite difficult to assess the relative importance of a suspected 'morphogen'. In contrast, in the cytogel model above, the 'morphogen'—if one insists on using that terminology—is one of the most common substances in biological systems: calcium. Moreover, its mode of action is not paradoxical; rather the model invokes only its well-documented

capacity to regulate actomyosin assembly and contractility. Indeed, both the mesenchymal and epithelial models simply reflect the laws of mechanics as applied to biological materials—cells and their extracellular environment. All of the model parameters are, in principle, independently measurable.

We emphasize that these models are only the first attempts to pursue a different line of investigation into biological pattern formation and morphogenesis. Deeper mathematical and numerical analysis will be necessary to investigate the models' potential for explaining biological phenomena, and undoubtably others will see how the models must be modified, or even changed in fundamental ways. Most importantly, we will consider the models successful, even if they are eventually proved incorrect, if they suggest experimental approaches to the study of morphogenesis that ultimately lead to the true explanation of one of biology's deepest mysteries.

References

COHEN, D. S., & MURRAY, J. D. 1981 A generalized model for growth and dispersal in a population. *J. Math. Biol.* **12,** 237–249.

DAVIDSON, D. 1981 The mechanism of feather pattern development in the chick I: The time of determination of feather position. II: Control of the sequence of pattern formation. *J. Embryol. exp. Morph.* **74,** 245–273.

GOODWIN, B. C., MURRAY, J. D., & BALDWIN, D. 1984 Calcium: the elusive morphogen in *Acetabularia*? (to appear).

HARRIS, A., STOPAK, D., & WILD, P. 1981 Fibroblast traction as a mechanism for collagen morphogenesis. *Nature* **290,** 249–251.

HARRIS, A., WILD, P., & STOPAK, D. 1980 Silicone rubber substrata: a new wrinkle in the study of cell locomotion. *Science* **208,** 177–179.

HUDSPETH, A. J. 1983 The hair cells of the inner ear. *Scientific American* **248,** 86–93.

MEINHARDT, H. 1982 *Models of Biological Pattern Formation.* New York: Academic Press.

MURRAY, J. D. 1977 *Nonlinear Differential Equation Models in Biology.* Oxford: Clarendon Press.

MURRAY, J. D. 1979 A pattern formation mechanism and its application to mammalian coat markings. '*Vito Volterra*' *Symposium on Mathematical Models in Biology,* Accademia dei Lincei, Rome, Dec. 1979 in *Lecture Notes in Biomathematics* **39,** pp. 360–399, Berlin: Springer-Verlag.

MURRAY, J. D. 1981*a* A pre-pattern formation mechanism for animal coat markings. *J. theor. Biol.* **88,** 161–199.

MURRAY, J. D. 1981*b* On pattern formation mechanisms for lepidopterian wing patterns and mammalian coat markings. *Phil. Trans. Roy. Soc. Lond.* **B295,** 473–496.

MURRAY, J. D., OSTER, G. F., & HARRIS, A. 1983 A mechanical model for mesenchymal morphogenesis. *J. Math. Biol.* **17,** 125–129.

MURRAY, J. D. & OSTER, G. F. 1984 Cell traction models for generating pattern and form in morphogenesis. *J. Math. Biol.* (in press).

ODELL, G., OSTER, G., BURNSIDE, B., & ALBERCH, P. 1981 The mechanical basis for morphogenesis I: Epithelial folding and invagination. *Devl. Biol.* **85,** 446–462.

OKUBO, A. 1980 *Diffusion and Ecological Problems: Mathematical Models.* Berlin: Springer-Verlag.

OSTER, G. F., MURRAY, J. D., & HARRIS, A. 1983 Mechanical aspects of mesenchymal morphogenesis. *J. Embryol. exp. Morph.* **78,** 83–125.

OSTER, G. F., MURRAY, J. D., & ODELL, G. M. 1984 Patterns of stereocillia and microvilli on hair cells of the inner ear. (To appear).

OSTER, G. F., & ODELL, G. M. 1984 The mechanochemistry of cytogels. In *Fronts, Interfaces and Patterns,* (BISHOP, A., Ed.) North Holland publ. Elsevier Science Div. (in press).

OSTER, G. F., & PERELSON, A. 1984*c* On the crawling of cells: a model for lamellipodia. (To appear).

OSTER, G. F. & PERELSON, A. 1984*c* On the crawling of cells: a model for lamellipodia. (To appear).

OTHMER, H. G. 1969 Interactions of reaction and diffusion in open systems. Ph.D. thesis. Chem. Eng. Dept., Univ. of Minnesota.

PENROSE, R. 1979 The topology of ridge systems. *Ann. Hum. Genet.* **42,** 435–444.

SENGEL, P. 1976 *Morphogenesis of Skin.* Cambridge: Cambridge University Press.

TRINKAUS, J. P. 1983 *Cells into Organs.* Englewood Cliffs: Prentice Hall.

TURING, A. M. 1952 The chemical basis of morphogenesis. *Phil. Trans. Roy. Soc.* (*Lond.*), **B237,** 37–72.

WESSELLS, N. (1977) *Tissue Interactions in Development.* Menlo Park: W. A. Benjamin.